PERGAMON

International Journal of Heat and Mass Transfer 43 (2000) 2883–2894

International Journal of HEAT and MASS TRANSFER

www.elsevier.com/locate/ijhmt

Heat and mass transfer modeling during the formation and ascension of superheated bubbles

F.B. Campos, P.L.C. Lage*

Programa de Engenharia Química, COPPE/UFRJ CEP 21.945-970, C.P. 68502, Rio de Janeiro, Brazil

Received 21 May 1999; received in revised form 15 October 1999

Abstract

A previously developed model for the heat and mass transfer of a single superheated bubble during the ascension stage was extended to include the formation stage. It allows variable properties and bubble radius changes, solving the gas conservation equations coupled to a bubble dynamics model. Its results were used to predict the existing experimental data in a direct contact evaporator with good agreement. A correction factor for isothermal gas hold-up correlations can be fully calculated by the model enabling good prediction of gas hold-up. The constant property assumption overestimates the gas hold-up and should not be used. Experimental data for steam bubbling process could be reasonably simulated using the superheated bubble model with some additional assumptions.

1. Introduction

Direct contact evaporation consists of liquid vaporization that occurs when kept in contact with a superheated gas without an intervening wall. This is usually carried out in a shallow bubble column operated nonisothermally and can be used for several applications [1]. The heat and mass transfer processes occur simultaneously, heating and vaporizing the liquid phase, whose vapor leaves the column carried by the bubbles. Due to the small gas hold-up values prevailing in direct contact evaporators, the process may be analyzed through the solution of the simultaneous heat and mass transfer problem in a single superheated bubble [2]. For the simulation and design of a direct contact evaporator, the bubble formation frequency and the vaporized mass per bubble must be estimated.

Each bubble is formed at a submerged orifice, detaches and then ascends through the continuous liquid phase. For conditions without heat or mass transfer, there exist several bubble formation models [3–5] that can estimate the bubble size at detachment and the corresponding bubble frequency. However, in our knowledge, there is no model for the simultaneous heat and mass transfer during the formation of superheated bubbles that can estimate both, the bubble formation frequency and the vaporized mass per bubble. There are some approximated analytical solutions that assume a mean value for the bubble radius [6] or its transient behavior [7]. They can estimate the heat and mass transfer during bubble formation only for a given bubble frequency and formation size.

The ascension stage is characterized by the bubble residence time which is determined from the ascension velocity and column height. The ascension velocity may be calculated from the bubble force

* Corresponding author. Tel.: +55-21-590-2241; fax: +55-21-290-6626.

E-mail address: paulo@peq.coppe.ufrj.br (P.L.C. Lage).

0017-9310/00/$ - see front matter
PII: S0017-9310(99)00344-0

Nomenclature

a coefficient in rule for constant property evaluation
A dimensionless constant ($R_{F_{hyp}} U^{t}_{F_{hyp}}/\alpha_{ref}$)
B transfer number ($C_{p_{ref}}(T_R - T_I)/L_1$)
Bi Biot number ($hR_{F_{hyp}}/\lambda_{ref}$)
c dimensionless mixture heat capacity ($C_p/C_{p_{ref}}$)
c_i dimensionless mean specific heat of component i ($\overline{C_{p_i}}^{0}/C_{p_{ref}}$)
C_D drag coefficient
C_P specific heat at constant pressure ($\sum_{i=1}^{2} Y_i \overline{C_{p_i}}^{0}$)
C_{p_i} specific heat of component i at constant pressure
D mass diffusion coefficient
f frequency of bubble formation
g gravity
G dimensionless gravity ($gR^2_{F_{hyp}}/\alpha_{ref} U^{t}_{F_{hyp}}$)
h heat transfer coefficient
H specific enthalpy
L latent heat of vaporization
Le Lewis number (α/D)
m evaporated mass per bubble
m_d mass of displaced liquid
m_g mass of gas inside the bubble
$\dot{m}$ bubble vaporization rate
M mass flow rate
$\dot{M}$ evaporator vaporization rate
N number of orifices
P system pressure
q diffusive heat flux
Q volumetric flow rate
r radius coordinate
R radius
S superficial area
t time
T temperature
T_R reference temperature for θ definition ($T_R = T_L$ when $T_I \neq T_L$)
U bubble ascension velocity
v radial velocity
V volume
Y mass fraction
z axial coordinate
Z bubble column height
W radial diffusion velocity

Greek symbols
α thermal diffusivity
β dimensionless radius ($R(t)/R_{F_{hyp}}$)
γ dimensionless density (ρ/ρ_{ref})
Γ dimensionless vaporization rate ($\dot{m}/4\pi R_{F_{hyp}} \rho_{ref} \alpha_{ref}$)
δ unit impulse function (Dirac delta function)
ε gas hold-up
ζ dimensionless axial coordinate ($z/R_{F_{hyp}}$)
η dimensionless radial coordinate ($r/R(t)$)
θ dimensionlesstemperature ($(T - T_I)/(T_R - T_I)$)
κ dimensionless thermal conductivity (λ/λ_{ref})
λ thermal conductivity
ρ density
τ dimensionless time ($\alpha_{ref} t/R^2_{F_{hyp}}$)
ϑ dimensionless radial velocity ($R_{F_{hyp}} v/\alpha_{ref}$)
ϕ dimensionless temperature ($(T - T_L)/(T_I - T_L)$)
Φ dimensionless injected mass rate ($\rho_I Q_I/4\pi R_{F_{hyp}} \rho_{ref} \alpha_{ref}$)
ψ dimensionless mass diffusion coefficient (D/D_{ref})
ω dimensionless bubble ascension velocity ($U/U^{t}_{F_{hyp}}$)

Subscripts
eff effective property
exp experimental
F bubble formation
g gas
hyp hypothetical bubbling process
i species i (1 for water vapor)
I injected gas
L liquid
orif orifice
r residence (at the end of bubble ascension)
ref reference state to evaluate physical properties for dimensionless variable definitions
S surface

Superscripts
– mean property
0 pure component
t terminal velocity

balance, using a correlation for the drag coefficient [8,9], from an empirical correlation for the bubble swarm velocity [10], or even from the definitions of the gas hold-up and superficial velocity [11]. A population correction factor [12], which depends on the gas hold-up, is needed for large gas hold-up values. The column height also depends on the gas hold-up, which is considerably overestimated by isothermal correlations [13–15].

Most existing heat and mass transfer models [15–18]

consider these processes only during the bubble ascension stage, even though there is some experimental evidence that most of the bubble superheat is transferred during its formation [19]. Moreover, the importance of the effects of bubble contraction and variable physical properties on the simultaneous heat and mass transfer during bubble ascension has been shown only recently [18]. In that work, a simplified correction factor has also been developed in order to apply isothermal gas hold-up correlation to predict gas hold-up in non isothermal systems. Comparison with experimental data in a direct contact evaporator has shown good agreement for the vaporization rate, but a larger discrepancy for the gas hold up in the column [18].

This work extends the previous model with variable gas-phase properties [18] to include the formation as well as the ascension of a superheated bubble, incorporating inlet gas source terms in the gas-phase conservation equations and coupling them to a bubble dynamics model. This allows the evaluation of the constant property assumption and the importance of the heat and mass transfer during the formation stage. Experimental data in a direct contact evaporator and in a steam bubbling process at elevated pressures have been compared to their simulated results. The agreement was very good for the direct contact evaporator data and reasonable interpretation of the data could be achieved for the steam bubbling process.

2. The superheated bubble model

Several hypotheses have been used to simplify the simulation of the heat and mass transfer process during the formation of a superheated bubble at a submerged orifice and its ascension through the liquid column. The superheated bubble model consists of a gas-phase heat and mass transfer model coupled to a bubble dynamics model, a description of the heat and mass transfer in the liquid phase and an interface equilibrium model, which are described in the following.

2.1. Gas-phase heat and mass transfer model

The bubble is assumed to be spherical with spherical symmetry for all field variables. In order to simulate the formation stage, it is postulated that a spherical residual bubble is formed at the orifice at the inlet gas conditions, which grows radially during the formation stage. The gas injected in the bubble is modeled through a source located at the bubble center which emits gas at the inlet conditions. Besides, the hydrostatic liquid column head is neglected in order to consider the pressure inside the bubble constant during the process, which is reasonable for the small column heights usually employed in direct contact evaporators. Other hypotheses are: the gas phase is an ideal binary mixture of water vapor and air (or any other pseudo-component), there is liquid–vapor equilibrium at the bubble surface, the viscous dissipation is negligible, the gravity is the only existing field force, and bubble formation is assumed to occur in the constant flow rate regime [20].

Using the above hypotheses, the gas phase model consists of the continuity, energy and chemical species conservation equations [21] in the form of a one-dimensional transient problem with moving boundaries. The momentum conservation equation is eliminated from the model by the assumption of constant pressure. Consider V_I to be the finite volume of the injection source situated at the center of the bubble, bounded by a surface of area S_I, and let S to be the bubble superficial area. The mass and energy source terms in the conservation equations are generated through a limit process, where, firstly, the conservation equations are integrated in the volume bounded by S_I and S, and then, V_I is taken to be zero under the assumption of no accumulation of heat and mass in the injection volume. This procedure expresses the gas injection as a point source of mass and energy at the bubble center. The resulting conservation equations for the bubble are

$$\frac{\partial \rho}{\partial t} + \frac{1}{r^2}\frac{\partial}{\partial r}\left(r^2 \rho v\right) = \rho_I Q_I \delta(r) \tag{1}$$

$$\frac{\partial}{\partial t}(\rho Y_i) + \frac{1}{r^2}\frac{\partial}{\partial r}\left[r^2 \rho Y_i (v + W_i)\right] = \rho_I Y_{i_I} Q_I \delta(r) \tag{2}$$

$$\frac{\partial}{\partial t}(\rho H) + \frac{1}{r^2}\frac{\partial}{\partial r}\left[r^2 (\rho v H + q)\right] = \rho_I Q_I H_I \delta(r) \tag{3}$$

where, for a binary ideal-gas mixture, the specific enthalpy, the conductive heat flux and the diffusion velocity of each species are, respectively, given by

$$H(T) = \sum_{i=1}^{2} Y_i H_i^0(T) \tag{4}$$

$$q = -\lambda \frac{\partial T}{\partial r} + \sum_{i=1}^{2} \rho H_i^0 Y_i W_i \tag{5}$$

$$W_i = -\frac{D_i}{Y_i}\frac{\partial Y_i}{\partial r} \tag{6}$$

The boundary conditions for Eqs. (1)–(3) at the bubble surface are given by mass and energy surface balances, being the same deduced in [18]. For the sake of completeness, they are given below.

$$-\frac{\dot{m}}{4\pi R^2} = \rho_s\left(v_s - \frac{dR}{dt}\right) \quad \text{at } r = R(t) \tag{7}$$

$$\rho_s D_s \frac{\partial Y_1}{\partial r}\bigg|_{r=R(t)} = \frac{\dot{m}}{4\pi R^2}\left(1 - Y_{1_s}\right) \quad \text{at } r = R(t) \tag{8}$$

$$-\lambda\frac{\partial T}{\partial r}\bigg|_{r=R(t)} = \frac{\dot{m}}{4\pi R^2}L_1(T_s) + h(T_s - T_L) \quad \text{at } r = R(t) \tag{9}$$

Since the specific heats of the gas-phase components do not depend strongly on temperature, constant mean specific heats for these pure substances, $\overline{C_{p_i}}^0$, can be used over the whole domain of temperature. Thus, Eq. (3) can be transformed into

$$\frac{\partial}{\partial t}(\rho C_p T) + \frac{1}{r^2}\frac{\partial}{\partial r}\left(r^2\rho v C_p T\right) - \frac{1}{r^2}\frac{\partial}{\partial r}\left(r^2\lambda\frac{\partial T}{\partial r}\right) - \left(\overline{C_{p_1}}^0 - \overline{C_{p_2}}^0\right)\frac{1}{r^2}\frac{\partial}{\partial r}\left(r^2 T\rho D\frac{\partial Y_1}{\partial r}\right) - \rho_I Q_I \delta(r)\sum_{i=1}^{2} Y_{i_I}\overline{C_{p_i}}^0 T_I = 0 \tag{10}$$

Since pressure is assumed to be constant in the model, the velocity profile inside the bubble is a consequence of bubble dilation or contraction, and it can be calculated from the continuity equation [22]. The radial integration of (1) gives

$$v(r,t) = -\frac{1}{r^2\rho(r,t)}\int_0^r \frac{\partial\rho(\xi,t)}{\partial t}\xi^2\,d\xi + \frac{\rho_I Q_I}{4\pi r^2\rho(r,t)} \tag{11}$$

where the contributions due to bubble dilation and gas injection are shown in the right-hand side.

It can be shown that the first term in Eq. (11) vanishes when r tends to zero. Thus, for the ascension stage, Q_I vanishes and the radial velocity is zero at the bubble center. On the other hand, during the formation stage, the finite flow rate Q_I should pass through an infinitesimal area around the center of the bubble, resulting in an infinite velocity. The usage of a staggered grid, as explained in Section 4, overcomes this difficulty.

2.2. Liquid phase and interface models

Since the liquid phase is assumed to be pure water, no mass transfer occurs in it and the heat transfer modeling is restricted to the evaluation of the heat transfer coefficient used in Eq. (9). In this work, the bubble-liquid heat transfer coefficient was estimated by the heat and mass transfer analogy using the Calderbank and Moo-Young correlation for the mass transfer from small bubbles [23]. Moreover, as the gas is considered ideal, the interfacial equilibrium can be determined from Raoult's law using Wagner's equation to calculate the water vapor pressure [24].

2.3. Bubble dynamics model

Bubble dynamics is affected by the heat and mass transfer processes due to bubble mass and volume changes, which, in turn, modify bubble formation and residence times, which affects the heat and mass transfer process, making the problem fully coupled. Thus, a bubble dynamics model must be added to the heat and mass transfer model for both the formation and ascension stages. Using the same simplifications originally made by Davidson and Schüler [3,4] (low pressure and gas flow rate values, spherical bubble, quiescent liquid, no effect of previous formed bubble on new forming bubble, negligible gas momentum and one-dimensional trajectory), the force balance and bubble position equations during the formation stage are given by:

$$\frac{dz}{dt} = U \tag{12}$$

$$\frac{11}{16}\left(\frac{dU}{dt} + 3\frac{U}{R}\frac{dR}{dt}\right) = g \tag{13}$$

The bubble grows up and accelerates, starting from rest ($t = 0$, $z = 0, U = 0$), until the detachment criterion ($z = R + R_{orif}$, $t = t_F$) is reached, when the ascension stage begins. During the ascension stage, the force balance becomes

$$\left(m_g + \frac{1}{2}m_d\right)\frac{dU}{dt} + \left(\frac{dm_g}{dt} + \frac{1}{2}\frac{dm_d}{dt} + \frac{\pi}{2}R^2\rho_L U C_D\right)U = \frac{4}{3}\pi R^3(\rho_L - \bar{\rho}_g)g \tag{14}$$

where the gas and displaced liquid momenta are considered. The initial conditions for the ascension stage are equivalent to the conditions at the end of the formation stage ($z = R + R_{orif}$, $t = t_F$, $U = U_F$) and the process ends at the top of the liquid column ($z = Z$, $t = t_r$, $U = U_r$).

The drag coefficient, C_D, has been calculated through Karamanev's correlation [9], using the liquid properties evaluated at the bulk liquid temperature, except for the viscosity and the surface tension, which are calculated at the film temperature. Due to the small gas hold-up values observed in direct contact evaporators, no population correction factor is applied to the ascension velocity.

The coupling of the bubble dynamics model to the heat and mass transfer model allows the predictions of

the bubble formation volume, the bubble formation frequency and the bubble ascension velocity under heat and mass transfer conditions, which, to the knowledge of the authors, has not been done before.

2.4. Physical property evaluation

Correlations for the specific heat, dynamic viscosity and thermal conductivity of air and water developed in [25], based on experimental data [26], have been used in this work. The density of the gas mixture was calculated by the ideal gas law. The gas mixture specific heat was obtained from the ideal solution behavior and the mixture thermal conductivity was estimated by the Wassiljewa's equation [24]. Correlations for the water latent heat of vaporization and for air–water vapor binary diffusion coefficient was also derived from Lage and Rangel's [25] work. The mean specific heat for each component was obtained from its definition, using the gas inlet and the liquid temperatures as the limits of integration:

$$\overline{C_{\mathrm{p}_i}}^{\,0} = \frac{1}{T_{\mathrm{I}} - T_{\mathrm{L}}} \int_{T_{\mathrm{L}}}^{T_{\mathrm{I}}} C_{\mathrm{p}_i}^{\,0}\, \mathrm{d}T \tag{15}$$

3. Gas hold-up in nonisothermal systems

The correlations commonly used to predict the gas hold-up in isothermal systems [13,14] fail when they are applied to nonisothermal bubble columns. The lower gas hold-up values observed in nonisothermal systems, such as in the direct contact evaporators [15], could be explained through the heat and mass transfer during the bubble formation and ascension stages that affects bubble volume, frequency of formation and residence time. In a previous work [18], the idea of incorporating a correction factor for nonisothermal conditions to well-know isothermal gas hold-up correlations has been developed. The basic idea is to use a superheated bubble model to calculate the total gas volume in the bubble column with and without the heat and mass transfer process. The latest case is a hypothetical bubbling process which corresponds to the gas holp-up estimates given by the isothermal correlations. The correction factor is calculated through [18]:

$$\frac{\varepsilon}{1-\varepsilon} = \left(\frac{\bar{\beta}}{\bar{\beta}_{\mathrm{hyp}}}\right)^3 \frac{f_{\mathrm{orif}}\, t_{\mathrm{r}}}{f_{\mathrm{orif}_{\mathrm{hyp}}}\, t_{\mathrm{r}_{\mathrm{hyp}}}} \frac{\varepsilon_{\mathrm{hyp}}}{1-\varepsilon_{\mathrm{hyp}}} \tag{16}$$

where

$$\bar{\beta} = \frac{1}{\zeta_{\mathrm{r}}} \int_0^{\zeta_{\mathrm{r}}} \beta(\zeta)\, \mathrm{d}\zeta \tag{17}$$

is the mean dimensionless bubble radius along the process. For not too shallow columns, it is possible to use the final values of β, β_{r}, in the place of $\bar{\beta}$ to obtain an approximated value for the correction factor. Eq. (16) is a slight modification of the form given in [18], because $\bar{\beta}_{\mathrm{hyp}} \neq 1$ when the bubble formation is considered in the integration of (17).

The superheated bubble model can be used to calculate the bubble formation frequency, its residence time and mean equivalent diameter, during the formation and ascension stages, for the nonisothermal and the hypothetical process, without heat and mass transfer.

4. Numerical procedure

The free boundary problem given by Eqs. (1), (2) and (10) and their boundary conditions, Eqs. (7)–(9), has been transformed into a fixed domain through the definition of a new radial coordinate, η, and a new dimensionless radius, β, to simplify the numerical solution. The conservation equations and their boundary conditions can be written in the following dimensionless form

$$\frac{\partial \gamma}{\partial \tau} - \frac{\eta}{\beta}\frac{\mathrm{d}\beta}{\mathrm{d}\tau}\frac{\partial \gamma}{\partial \eta} + \frac{1}{\eta^2\beta}\frac{\partial}{\partial \eta}\left(\eta^2 \gamma \vartheta\right) - \frac{4\pi}{\beta^3}\Phi\delta(\eta) = 0 \tag{18}$$

$$\begin{aligned}\frac{\partial}{\partial \tau}(\gamma Y_1) - \frac{\eta}{\beta}\frac{\mathrm{d}\beta}{\mathrm{d}\tau}\frac{\partial}{\partial \eta}(\gamma Y_1) + \frac{1}{\eta^2\beta}\frac{\partial}{\partial \eta}\Bigg[\eta^2\gamma\Bigg(Y_i\vartheta \\ - \frac{\psi}{\beta Le_{\mathrm{ref}}}\frac{\partial Y_1}{\partial \eta}\Bigg)\Bigg] - \frac{4\pi}{\beta^3}\Phi\delta(\eta)Y_{1_{\mathrm{I}}} = 0\end{aligned} \tag{19}$$

$$\begin{aligned}\frac{\partial}{\partial \tau}(\gamma c\theta) - \frac{\eta}{\beta}\frac{\mathrm{d}\beta}{\mathrm{d}\tau}\frac{\partial}{\partial \eta}(\gamma c\theta) + \frac{1}{\eta^2\beta}\frac{\partial}{\partial \eta}\Bigg[\eta^2\Bigg[\gamma c\theta\vartheta \\ - \frac{\kappa}{\beta}\frac{\partial \theta}{\partial \eta}\Bigg)\Bigg] - (c_1 - c_2)\frac{1}{\eta^2\beta}\frac{\partial}{\partial \eta}\left(\eta^2\frac{\gamma\psi\theta}{Le_{\mathrm{ref}}\beta}\frac{\partial Y_1}{\partial \eta}\right) \\ - \frac{4\pi}{\beta^3}\Phi\delta(\eta)\sum_{i=1}^{2} Y_{i_{\mathrm{I}}} c_i \theta_{\mathrm{I}} = 0\end{aligned} \tag{20}$$

$$-\frac{\Gamma}{\beta^2} = \gamma_{\mathrm{s}}\left(\vartheta_{\mathrm{s}} - \frac{\mathrm{d}\beta}{\mathrm{d}\tau}\right), \quad \eta = 1 \tag{21}$$

$$\left.\frac{\gamma_s \psi_s \beta}{Le_{ref}} \frac{\partial Y_1}{\partial \eta}\right|_{\eta=1} = \Gamma\left(1 - Y_{1_s}\right), \quad \eta = 1 \tag{22}$$

$$\left.-\frac{\kappa}{\beta} \frac{\partial \theta}{\partial \eta}\right|_{\eta=1} = \frac{\Gamma}{\beta^2 B} + Bi(\theta_s - \theta_L), \quad \eta = 1 \tag{23}$$

For the formation stage, the bubble dynamics model are given in dimensionless forms by

$$\frac{d\omega}{d\tau} + 3\frac{\omega}{\beta}\frac{d\beta}{d\tau} - \frac{16}{11}G = 0 \tag{24}$$

$$\frac{d\zeta}{d\tau} - A\omega = 0 \tag{25}$$

where the initial conditions are $\tau = 0$, $\zeta = 0$, $\omega = 0$, and the detachment criterion is given by $\zeta = \beta + \beta_{orif}$ at $\tau = \tau_F$. For the ascension stage, the dimensionless force balance is given by

$$\frac{1}{6}\left(2\bar{\gamma}_g + \gamma_L\right)\frac{d\omega}{d\tau} + \left[\gamma_s\left(\frac{d\beta}{d\tau} - \omega_s\right) + \frac{\gamma_L}{2}\frac{d\beta}{d\tau} + \frac{A}{8}\gamma_L \omega C_D\right]\frac{\omega}{\beta} - \left(\gamma_L - \bar{\gamma}_g\right)\frac{G}{3} = 0 \tag{26}$$

whose initial conditions are those at the bubble detachment and the ascension stage finishes at $\zeta = \zeta_r$, $\tau = \tau_r$, $\omega = \omega_r$.

The numerical model given by Eqs. (18)–(23) has been solved by the method of lines using finite-volume spatial discretization. Eqs. (19) and (20) have been discretized in η-coordinate using a staggered nonuniform grid, where the velocity grid points are placed at the volume interfaces. The power-law interpolation function given by Patankar [27] was used to evaluate the convective–diffusive terms. When it was necessary, this scheme was slightly modified to calculate the values of the dependent variables at the volumes interfaces. The terms where $d\beta/d\tau$ appears explicitly and the interdiffusion term in the energy equation have been incorporated in the source terms of the discretization scheme [27]. The boundary conditions given by Eqs. (22) and (23) and the symmetry conditions at the bubble center can be directly incorporated in the discretized equations. The integration of Eq. (18) over the η-coordinate allows the calculation of the dimensionless radial velocity profile inside the bubble as soon as the dimensionless temperature and concentration profiles are calculated during the simulation. The resulting system of nonlinear ordinary differential equations and the dynamic model, Eqs. (24)–(26), have been numerically integrated using the DASSL routine [28], with automatic error control. Typically, an absolute tolerance of 10^{-8} and a relative tolerance of 10^{-6} are used in the mixed tolerance convergence criterion of DASSL. Eq. (17) was integrated using the trapezoidal rule in order to determine $\bar{\beta}$. The mass of vaporized water per bubble, m, is also calculated through trapezoidal integration along the transient simulation. Enough time intervals are taken to obtain these values with an accuracy greater than 1%. The dimensionless mean value of the gas density in the bubble volume, $\bar{\gamma}_g$, is obtained through a simple integration using the control volume density values.

5. Results and discussion

The numerical implementation of the superheated bubble model allows the simulation of three different models. The first one, called Model I, is the superheated bubble model for the formation and the ascension stages. The solution of bubble dynamics coupled to the heat and mass transfer model makes Model I capable of predicting the bubble volume at detachment, and its frequency of formation. The second model, called Model II, is also valid for the formation and ascension stages but it ignores the heat and mass transfer effect on the bubble formation volume. In this case, the detachment is supposed to occur when the bubble volume is that predicted by a pure dynamical model [3,4] ($R = R_{F_{hyp}} + R_{orif}$), leading to a formation frequency that can be different from that predicted by the pure dynamical model. During the ascension stage, it is supposed that the bubble assumes instantaneously its terminal velocity, as given by Karamanev correlation [9]. The last model, called Model III, ignores completely the bubble formation, assuming that the bubble is instantaneously formed at the final bubble volume as predicted by a pure dynamical model (Davidson and Schüler model [3,4]), with no effects of the heat and mass transfer process. Thus, the initial bubble volume and the formation frequency are equal to those for the hypothetical bubbling process. Model III corresponds to the model developed in our previous work [18].

Table 1 gives the simulation conditions used to obtain the results presented in Tables 2 and 3 and in Fig. 1. In this table, Cases 1–5 use the same mass flow rate of gas through the orifice and the same orifice diameter, which has been made very small, in order that the spherical bubble approximation be adequate. Cases 6 and 7 are related to the experimental direct contact evaporator data of Queiroz [15]. The values of the bubble formation radius for the hypothetical bubbling process without heat and mass transfer, $R_{F_{hyp}}$, calculated by the Davidson and Schüler model [3,4], are also shown in Table 1.

Case 1 was used for a consistency check of the numerical model, where the gas is at the equilibrium con-

Table 1
Conditions for simulations

Case	T_I (K)	T_L (K)	Y_{l_I} (%)	M_{orif} (mg/s)	Q_{orif} (cm^3/s)	R_{orif} (mm)	$R_{F_{byp}}$ (mm)
1	323	323	7.97	1.038	1.000	0.10	1.76
2	900	323	1.96	1.038	2.689	0.10	2.61
3	900	353	1.96	1.038	2.689	0.10	2.61
4	400	323	1.96	1.038	1.793	0.10	2.22
5	400	353	1.96	1.038	1.793	0.10	2.22
6	1066	350	7.59	17.90	56.78	0.65	8.88
7	742	350	7.59	17.90	39.52	0.65	7.70

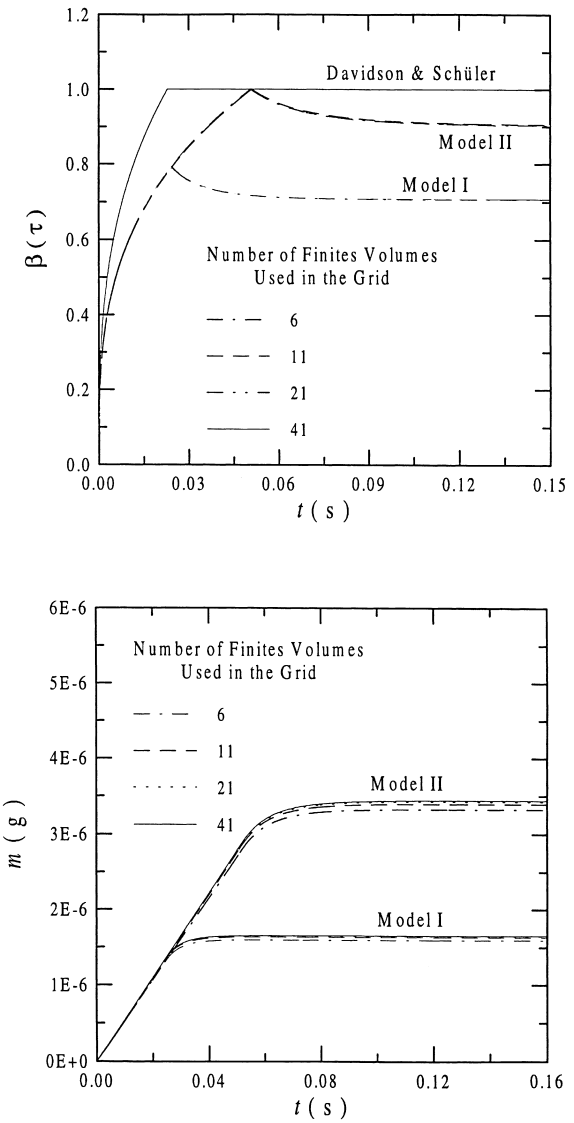

Fig. 1. Convergence analysis during the bubble formation and ascension for Model I ($t_F = 24$ ms, $\tau_F = 0.51$) and for Model II ($t_F = 51$ ms, $\tau_F = 1.06$): (a) dimensionless radius and (b) mass of vaporized water.

ditions, leading to simulations with no change in temperature and water concentration profiles during the process, as physically expected. The numerical model was also checked by comparing its results with those of another numerical model that had been previously developed for droplet vaporization, using the orthogonal collocation method [29]. Both models were slightly modified to solve a spherically symmetric moving-boundary heat transfer problem, with specified heat flux at the sphere surface and constant physical properties. Results for the transient behavior of the surface temperature for both models were in excellent agreement, validating the present numerical model.

Fig. 1 shows the convergence characteristics in a nonuniform grid of Models I and II in terms of the transient behavior of the dimensionless radius and the mass of vaporized water for the conditions of Case 2. Although 11 finite volumes seem to be enough to assure the convergence of these variables, a nonuniform grid with 81 finite volumes has been used to obtain all the results shown below, in order to guarantee convergence of the radial profiles of temperature and concentration. The peak that appears in the dimensionless radius transient profile represents the end of bubble formation stage, where the gas injection is instantaneously stopped as the bubble detaches the orifice. Fig. 1(a) also shows the transient behavior of the dimensionless bubble radius predicted by the Davidson and Schüler model [3,4]. Comparing the simulated results for Model I and Davidson and Schüler model, both with the same detachment criterion, it is clear that the heat and mass transfer process greatly affects bubble formation volume, whereas the bubble formation frequency is less affected. The results for Model II show clearly that the detachment criterion used by this model is not adequate.

Model I was used to analyze the effects of considering constant properties and the interdiffusion term in the energy conservation equation, as in our previous work [18]. It has been found that the interdiffusion term effect is negligible but the variable property effect is quite pronounced, affecting bubble size, water vaporization per bubble, bubble formation time and the tem-

Table 2
Gas hold-up and mass vaporization rate predictions

	Case	$\bar{\beta}$	β_r	t_r (s)	f_{orif} (s^{-1})	ε		m_r (10^{-7} kg)	f (10^6 h^{-1})	$\dot{M}$ (kg/h)
						A&Y[a]	H[b]			
Model I (variable properties)	6	0.792	0.782	1.295	20.36	0.058	0.054	2.91	21.1	6.15
	7	0.894	0.892	1.311	21.12	0.058	0.055	2.82	21.9	6.17
Model I (constant properties, $a = 1/2$ and ρ at $\bar{T}$ and $\bar{Y}_1$)	6	0.955	0.969	1.187	19.98	0.088	0.082	2.93	20.7	6.07
	7	0.994	1.008	1.250	20.97	0.075	0.071	2.79	21.7	6.07
Model I (constant properties, $a = 1/2$ and ρ at T_I and Y_{1_I})	6	1.090	1.108	1.114	18.78	0.089	0.085	4.39	19.5	8.57
	7	1.091	1.109	1.195	20.12	0.116	0.108	3.71	20.9	7.73
Model I (constant properties, $a = 1/3$ and ρ at $\bar{T}$ and $\bar{Y}_1$)	6	1.024	1.039	1.150	19.31	0.101	0.094	3.03	20.0	6.06
	7	1.047	1.062	1.217	20.49	0.083	0.079	2.85	21.2	6.07
Model II (variable properties)	6	0.872	0.863	2.015	15.08	0.086	0.080	3.93	15.6	6.14
	7	0.934	0.932	2.076	18.49	0.089	0.084	3.22	19.2	6.17
Model II (constant properties, $a = 1/2$ and ρ at $\bar{T}$ and $\bar{Y}_1$)	6	1.035	1.047	1.848	15.83	0.131	0.123	3.70	16.4	6.06
	7	1.043	1.054	1.964	18.38	0.114	0.108	3.18	19.1	6.07
Model II (constant properties, $a = 1/3$ and ρ at $\bar{T}$ and $\bar{Y}_1$)	6	1.039	1.048	1.825	22.31	0.177	0.166	3.11	23.13	7.19
	7	1.046	1.054	1.952	23.40	0.141	0.135	2.79	24.26	6.78
Model III (variable properties)	6	0.820	0.809	2.064	19.34	0.091	0.085	3.24	20.1	6.50
	7	0.919	0.912	2.121	20.67	0.094	0.089	3.03	21.4	6.48
Model III (constant properties, $a = 1/3$ and ρ at T_1 and Y_{1_1})	6	1.097	1.099	1.794	19.34	0.172	0.162	3.59	20.1	7.22
	7	1.096	1.099	1.918	20.67	0.138	0.131	3.17	21.4	6.77
Hypothetical bubbling process	6	0.998	1.000	1.821	19.34	0.141	0.132	–	–	–
	7	0.998	1.000	1.955	20.67	0.112	0.107	–	–	–
Experimental	–	–	–	–	–	0.05 ± 0.03		–	–	5.6 ± 0.5

[a] Akita and Yoshida [13].
[b] Hikita et al. [14].

perature and concentration profiles, which is in agreement with the results previously obtained with Model III [18].

Simulations of Cases 2, 3, 4 and 5 have been carried out with Model I to verify how the disperse and continuous phase temperatures affect the mass of vaporized water. It has been found that a 300 K increase in the initial gas temperature leads to an increase of 8% in the mass of vaporized water, while a 30 K rise in the liquid temperature is responsible for a 730% increase in the mass of vaporized water. The gas phase temperature affects the vaporization mainly in the beginning of the process, where a larger temperature difference between the phases produces larger vaporization rates. This means that the gas inlet temperature is an important design variable only for direct contact evaporators with shallow columns.

The lack of available experimental data on direct contact evaporation has restrained our analysis to the Queiroz's experimental data [15], which was obtained using the direct contact evaporator unit in the Thermofluid Dynamics Laboratory at PEQ/COPPE. The evaporator diameter was 57 cm, and the gas distribution system was composed of 288 orifices of 1.3 mm diameter, each. The data on gas hold-up and water vaporization rate used here corresponds to the operational conditions that are characterized by Cases 6 and 7 in Table 1. In those cases, the mean liquid column height during mass vaporization measurement was 55.8 cm. Although Queiroz [15] has used combustion gas, the calculations shown in the following analysis have been carried out using the physical properties of a water vapor–air mixture. A comparison of specific heats at constant pressure and thermal conductivities for the different substances allows the estimation of the error involved in this approximation to be around 4%. The inlet gas temperature of 1066 K (Case 6) was measured by a thermocouple located approximately at 150 cm after the gas burner and about 80 cm ahead of the gas distribution system. Correction for thermal losses through the gas admission tube has led to the temperature 742 K (Case 7). Since the heat loss was estimated, the corrected temperature could be in error. Thus, simulations were performed using either the measured temperature or the corrected temperature.

In Table 2, Queiroz's experimental data for gas hold-up and global mass vaporization rate are compared to predictions obtained by using Models I, II and III, for the experimental conditions of Cases 6 and 7. The experimental errors shown for $\dot{M}$ and ε are basically due to the imprecision in water level measurements in the evaporator. The estimated values for $\dot{M}$ have been obtained by multiplying the predicted bubble formation frequency at an orifice by the number of orifices in the gas distribution system (giving the global bubble formation frequency, f) and by the predicted evaporated mass per bubble at the end of the process, m_r. The gas hold-up estimates are calculated by known isothermal correlations and Eq. (16) using the predicted values for β, t_r and f_{orif}. The values for the uncorrected (hypothetical bubbling process) and corrected gas hold-up using the Akita and Yoshida [13] (A&Y) and the Hikita et al. [14] (H) correlations are listed in Table 2. The dimensionless bubble radius at the end of the process, β_r, is also shown in Table 2 for the cases analyzed. Its values are practically equal to the $\bar{\beta}$ values due to the largest rates of heat and

Table 3
Heat transfer during the steam bubble formation in saturated water ($T_I - T_L = 150$ K)

	P (bar)	M_{orif} (g/min)	V_F (mm^3)	f_{orif} (s^{-1})	ϕ_F	ϕ_{orif}
Experimental data	40	3.0	150	32	0.35	0.88
		9.0	300	55	0.54	0.95
	80	3.0	72	32	0.41	0.83
		9.0	146	45	0.57	0.95
Simulation (Model I)	40	3.0	136	30	0.71	
		9.0	474	24	0.82	
	80	3.0	73	33	0.71	
		9.0	273	27	0.85	
Simulation (Model I with experimental frequency)	40	3.0	128	32	0.71	
		9.0	218	55	0.84	
	80	3.0	76	32	0.71	
		9.0	149	45	0.86	
Simulation (Model I with experimental frequency and $\lambda_{eff} = 20\lambda$)	40	3.0	122	32	0.35	
		9.0	212	55	0.53	
	80	3.0	75	32	0.40	
		9.0	149	45	0.59	

mass transfer that take place in the beginning of the process.

In order to show the importance of considering variable properties, Table 2 also lists some results obtained through simulations using constant properties, which have been evaluated at $\bar{T} = T_I - a(T_I - T_L)$ and $\bar{Y}_I = Y_{I_I} - a(Y_{I_I} - Y_I^*)$ where Y_I^* is the water vapor equilibrium concentration at T_L. Following [18], the arithmetic mean ($a = 1/2$) and the one-third rule ($a = 1/3$) have been used. For Model III with the constant property assumption, the gas density must be kept at the initial conditions to be consistent with the bubble formation model. On the other hand, for Models I and II with constant properties, the density may be either evaluated at the initial conditions or at the mean conditions. Both the conditions have been tested and some results are presented in Table 2. For comparison, previous results obtained with Model III with constant properties [18] are also shown in Table 2.

The Akita and Yoshida [13] and the Hikita et al. [14] correlations are the most commonly used for gas hold-up estimation in bubble columns. Originally developed for isothermal conditions, they fail to predict the value of the gas hold-up in nonisothermal bubble columns. Table 2 (hypothetical bubbling process) shows that the gas hold-up is overestimated by 100–180% by these correlations for the experimental conditions of Cases 6 and 7. The correction factor values predicted by all models with variable properties lead to smaller values for the gas hold-up, showing the trend for the heat and mass transfer effect in the present case. However, only Model I using variable properties is really successful in determining the gas hold-up for a nonisothermal system. Its gas hold-up prediction for Cases 6 and 7 using both correlations are within 16% of the experimental value, which is much smaller than the experimental error (60%). Using variable properties, the worst estimates for the gas hold-up are obtained with Model III, which is caused by the neglect of heat and mass transfer during the bubble formation stage [18].

The $\dot{M}$ results obtained for Cases 6 and 7 and using Models I and II with variable properties are all in good agreement with the experimental data, being basically within its experimental error. This shows that, in this case, the mass vaporization rate is quite insensitive to the gas inlet temperature and to the formation stage extension. Model III shows poorer results due to the neglect of the bubble formation stage. There are two possible explanations for the discrepancy in the experimental data and the $\dot{M}$ prediction by Model I with variable properties. Firstly, since the evaporator was not perfectly insulated, there should exist some condensation inside it which would led to a lower vaporization rate. Secondly, the inlet gas flow rate had a 10% measurement error. When a 10% reduction of the inlet gas flow rate is used in Model I with variable properties, it predicts that $\dot{M} =$ 5.5 kg/h, which agrees remarkably well with the experimental data. It should be noted that the corrected gas hold-up is practically not affected by this flow rate reduction. From the agreement obtained for the gas hold-up and mass vaporization rate, Model I (with variable properties) offers the best representation of the superheated bubble process for this direct contact evaporator data.

We now turn to the analysis of the constant property simulations. Comparing the results obtained using the constant property assumption for all models, it can be seen that there is no convenient rule for calculating the physical properties that leads to good predictions of both, ε and $\dot{M}$. Models I and II evaluating all properties at $\bar{T}$ and $\bar{Y}_I$ using $a = 1/2$ give good $\dot{M}$ predictions but too large values for ε (42–160% larger than the experimental value). The $a = 1/3$ rule leads to worse $\dot{M}$ and ε values for Models I and II, but better values for $\dot{M}$ using Model III [18]. The evaluation of ρ at the initial conditions in Models I and II has not affected the predicted $\dot{M}$ values, but the ε predictions have become worst.

In order to make a more rigorous test of Model I predictions, it has also been applied to simulate the experimental data obtained by Schmidt [19] for the heat transfer during the bubbling of superheated steam in saturated water at very high pressures. Due to the ideal gas hypothesis used in our model, only the data obtained for 40 and 80 bar have been simulated. Even for these conditions, a reasonable error is expected due to the nonideal gas behavior. The experimental conditions chosen to be simulated are those corresponding to bubble formation at a 3 mm diameter orifice through the injection of steam at mass flow rates of 3.0 and 9.0 g/min, which is kept at 150 K over the saturated water temperature. The experimental data for the bubble formation volume, V_F, bubble formation frequency, f_{orif}, the dimensionless temperatures of the inlet gas, ϕ_{orif}, and of the gas bubble at the end of formation, ϕ_F, are shown in Table 3. The inlet steam temperature was directly measured in the gas distribution chamber and it is somewhat lower than the steam temperature fed to the apparatus [19]. These dimensionless temperatures are a measure of the superheating level of the vapor. Thus, the fraction of the initial available vapor superheat that is transferred during the formation stage is estimated by $1 - \phi_F/\phi_{orif}$.

Model I with variable properties has been used to simulate the steam bubbling process described above, where the gas inlet temperature was calculated from the ϕ_{orif} values. Table 3 shows the simulated results for the bubble formation volume, frequency of formation and dimensionless bubble temperature at the end of

formation, ϕ_F, obtained with Model I, and a variant of Model I where the experimental frequency of formation has been used. This modification has been employed because the bubble dynamics model was not capable of predicting the corrected values for V_F and f_{orif} for the largest gas flow rate (9.0 g/min), although for the lowest flow rate (3.0 g/min), the prediction is quite good. The neglect of the gas momentum in the bubble formation model should be responsible for these inaccurate predictions. Simulations using the experimental frequency improves the V_F prediction for the largest mass flow rate with little effect on the other results.

The results obtained for ϕ_F using the experimental frequency are not in agreement with the experimental data. This can be caused partially by the pressure levels, where the ideal gas hypothesis is violated, and partially by the establishment of an effective mixing mechanism inside the bubble for the experimental conditions analyzed. These effects are not considered in the present model which has been developed to study direct contact evaporation. In order to verify if a mixing mechanism (circulation or turbulent mixing) is responsible for the discrepancies in model predictions, the concept of an effective thermal conductivity has been used. Table 3 also shows such results, where the effective thermal conductivity was assumed to be 20 times the gas conductivity. The simulated ϕ_F values are in very good agreement with all experimental data, and the increase in the thermal conductivity has hardly affected the bubble formation volume. This indicates that an effective mixing mechanism is in effect inside the bubble.

6. Conclusions

This work developed a superheated bubble model which consists of the mass and energy conservation equations inside the bubble coupled to a bubble dynamics model, taking into account variable physical properties in the gas phase. This model is able to simulate the formation and ascension stages of a superheated bubble, allowing the estimation of bubble detachment volume, bubble formation frequency and heat and mass transfer rates during the bubbling process.

Experimental data of gas hold-up and mass vaporization rate in a direct contact evaporator have been used to validate the model and analyze some of its hypotheses. The model is able to accurately predict gas hold-up and mass vaporization rate values. The gas hold-up estimates are obtained through a correction factor for nonisothermal systems, which is applied to isothermal gas hold-up correlations. It was shown that the heat and mass transfer process during bubble formation is responsible for the low gas hold-up values measured in nonisothermal bubble columns. The relevance of considering variable physical properties is also shown, becoming clear that the constant property assumption should not be used.

The model has also been used to interpret some experimental data on superheated steam bubble formation in saturated water at higher pressure. After imposing the experimental frequency of formation and an effective thermal conductivity to the model, it was capable of giving estimates in good agreement with the experimental data, showing that there should exist an effective mixing mechanism inside the bubble during its formation for the conditions analyzed.

Acknowledgements

The kind assistance of Prof. E.M. Queiroz in obtaining the raw experimental data is gratefully acknowledged. The authors also acknowledge the financial support obtained from CNPq, grant number 520660/98-6.

References

[1] D. Bharatahn, Direct contact evaporation, in: F. Kreith, R.F. Boehm (Eds.), Direct Contact Heat Transfer, Hemisphere, New York, 1988, pp. 203–222.
[2] P.L.C. Lage, C.M. Hackenberg, Simulation and design of direct contact evaporators, in: T.N. Veziroglu (Ed.), Multiphase Transport and Particulate Phenomena, vol. 2, Hemisphere, New York, 1990, pp. 577–592.
[3] J.F. Davidson, B.O.G. Schüler, Bubbles formation at an orifice in an inviscid liquid, Trans. Instn. Chem. Engrs 38 (1960) 335–342.
[4] J.F. Davidson, B.O.G. Schüler, Bubbles formation at an orifice in a viscous liquid, Trans. Instn. Chem. Engrs 38 (1960) 144–154.
[5] E.S. Gaddis, A. Vogelpohl, Bubbles formation in quiescent liquids under constant flow conditions, Chem. Engng. Sci 41 (1986) 97–105.
[6] A.D. Pinto, C.M. Hackenberg, Evaporação Interfacial Durante a Formação de Bolhas Superaquecidas em Orifícios, in: Proceedings of the 5th Brazilian Thermal Sciences Metting (ENCIT), ABCM, São Paulo, Brazil, vol. 1, 1994, pp. 36–44.
[7] C.M. Hackenberg, A.C. Mezavilla, Transient heat and mass transfer during the formation of superheated spherical bubbles, in: J. Padet, F. Arinç (Eds.), Transient Convective Heat Transfer — ICHMT, vol. 1, Begellhouse Inc, New York, 1996, pp. 409–420.
[8] R. Clift, J.R. Grace, M.E. Weber, Bubbles Drops and Particles, Academic Press, New York, 1978, pp. 111–116 and 204–207.

[9] D.G. Karamanev, Rise of gas bubbles in quiescent liquids, AIChE J 40 (1994) 1418–1421.
[10] J.F. Davidson, D. Harrison, in: Fluidized Particles, Cambridge University Press, Cambridge, 1963, p. 53.
[11] Y.T. Shah, B.G. Kelkar, S.P. Godbole, W.D. Deckwer, Design parameters estimations for bubble column reactors, AIChE J 28 (1982) 353–379.
[12] E. Ruckenstein, On mass transfer in the continuous phase from spherical bubbles or drops, Chem. Eng. Sci 19 (1964) 131–146.
[13] K. Akita, F. Yoshida, Bubble interfacial area and liquid-phase mass transfer coefficient in bubble columns, Ind. Eng. Chem. Proc. Des. Dev 13 (1974) 84–91.
[14] H. Hikita, S. Asai, K. Tanigawa, K. Segawa, M. Kitao, Gas hold-up in bubbles columns, Chem. Eng. Journal 20 (1980) 59–67.
[15] E.M. Queiroz, Transferĕncia Simultâanea de Calor e Massa em Processos de Borbulhamento, D.Sc. thesis, COPPE/UFRJ, Rio de Janeiro, Brazil, 1990.
[16] C.M. Hackenberg, A.L. Andrade, Transient surface temperature of superheated bubbles, in: T.N. Veziroglu (Ed.), Particulate Phenomena and Multiphase Transport, vol. 1, Hemisphere, Washington, 1988, pp. 377–382.
[17] E.M. Queiroz, C.M. Hackenberg, On the transient heat and mass transfer modelling of direct contact evaporators, in: J. Padet, F. Arinç (Eds.), In Transient Convective Heat Transfer — ICHMT, vol. 1, Begellhouse Inc, New York, 1996, pp. 179–189.
[18] F.B. Campos, P.L.C. Lage, Simultaneous heat and mass transfer during the ascension of superheated bubbles, Int. J. Heat Mass Transfer 43 (2000) 179–189.
[19] H. Schmidt, Bubble formation and heat transfer during dispersion of superheated steam in saturated water—II: from superheated steam bubbles to saturated water during bubble formation, Int. J. Heat Mass Transfer 20 (1977) 647–854.
[20] R. Kumar, N.R. Kuloor, The formation of bubbles and drops, Advances in Chemical Engineering 8 (1970) 255–367.
[21] K.K. Kuo, Principles of Combustion, Wiley, New York, 1986 (Chapter 3).
[22] P.L.C. Lage, R.H. Rangel, C.M. Hackenberg, Nonideal vaporization of a dilating binary droplet with variable properties, Int. J. Heat and Mass Transfer 36 (1993) 3731–3741.
[23] P.H. Calderbank, M.B. Moo-Young, The continuous phase heat and mass transfer properties of dispersions, Chem. Eng. Sci 16 (1961) 39–54.
[24] R.C. Reid, J.M. Praunitz, B.E. Poling, The Properties of Gases and Liquids, 4th ed., McGraw-Hill, New York, 1987 (Chapters 7 and 8).
[25] P.L.C. Lage, R.H. Rangel, On the role of internal radiation absorption in single droplet vaporization, Paper number AIAA-92-0106, AIAA, 1992.
[26] N.B. Vargaftik, Tables on the Thermophysical Properties of Liquids and Gases in Normal and Dissociated States, Wiley, New York, 1975.
[27] S.V. Patankar, Numerical Heat Transfer and Fluid Flow, McGraw-Hill, New York, 1980.
[28] Petzold, L.R., DASSL code, version 1989, L316, Computing and Mathematics Research Division, Lawrence Livermore National Laboratory, Livermore, 1989.
[29] P.L.C. Lage, R.H. Rangel, Single droplet vaporization including thermal radiation absorption, Journal of Thermophysics and Heat Transfer 7 (1993) 502–509.